ARTICLES

The Transformation of Nesquehonite to Hydromagnesite in the System CaO-MgO-H$_2$O-CO$_2$: An Experimental FT-Raman Spectroscopic Study

Laurence Hopkinson, Ken Rutt,[1] *and Gordon Cressey*[2]

*School of Environment and Technology, University of Brighton, Cockcroft Building,
Lewes Road, Brighton BN2 4GJ, United Kingdom440
(e-mail: l.hopkinson@brighton.ac.uk)*

ABSTRACT

This study reports the nature of the nesquehonite-to-hydromagnesite transition at 52°C in an aqueous medium hosting magnesian calcite and nesquehonite. The latter mineral occurs with abundant calcite at the floor of the experimental chamber (substrate) and as a film of needles at the interface between the mother liquor and atmosphere (surface film). The experimental vessel was held at 52°C for 336 h and at 60°C for a further 192 h. Precipitates were analyzed by Fourier transform (FT)–Raman, augmented by FT-infrared and x-ray diffraction. At 52°C, hydromagnesite and dypingite occur with abundant quantities of a hitherto unreported transitory magnesium hydrate carbonate (TMHC), together with huntite, magnesian calcite, and traces of nesquehonite and monohydrocalcite. The FT-Raman spectra of the first-formed hydromagnesite crystals contain the Raman forbidden v_2 mode, interpreted to indicate a relaxation in selection rules, caused by rapid precipitation. Hydromagnesite growth at the expense of TMHC was more advanced in the substrate than in the coexisting surface film. Additional heating at 60°C resulted in the loss of TMHC and emergence of a dypingite- and hydromagnesite-rich assemblage, with associated strengthening of selection rules. Transitory magnesium hydrate and hydroxyl carbonates and huntite formed during CO$_2$ degassing, fueled by the thermally driven decrease in solubility of CO$_2$ in water and the progressive dissolution of metastable phases. Advancement of the N→HM transition in the substrate most likely reflects greater Ca$^{2+}_{(aq)}$ availability to promote acid generation through calcite precipitation, thereby accelerating transitory-phase dissolution.

Introduction

Hydromagnesite is an abundant naturally occurring magnesium hydroxyl carbonate that constitutes a large and potentially reactive sink for C (e.g., Walling et al. 1995). The mineral is of significant importance in sedimentary geology and planetology (e.g., Königsberger et al. 1999; Russell et al. 1999; Edwards et al. 2005b). Accordingly, understanding possible biogenic and abiogenic origins of the mineral is of consequence. Allied to this is the recognized need for Raman spectroscopic studies of mixed calcium and magnesium carbonate assemblages as databases for extraterrestrial planetary exploration (Edwards et al. 2005a).

The magnesium trihydrate carbonate nesquehonite readily precipitates from solutions of magnesium bicarbonate at room temperature. It is metastable and loses its CO$_2$ slowly at near-surface ambient temperatures in the air and under water and converts readily to hydromagnesite (e.g., Kazakov et al. 1959). This process is accelerated significantly at higher temperatures, with transformation to hydromagnesite occurring in an aqueous medium by dissolution-precipitation step(s) at reported temperatures of 52°–65°C (Langmuir 1965; Davies and Bubela 1973; Botha and Strydom 2001). The precise details of the transformation process and the character of the transitory mineral and/or mineraloid phase(s) remain unclear (fig. 1), although it seems certain that at least some naturally occurring hydromagnesite originates from the instability of the nesquehonite-to-hydromagnesite transformation (Davies and Bubela 1973).

Naturally occurring magnesium-enriched aqueous solutions overwhelmingly contain at least
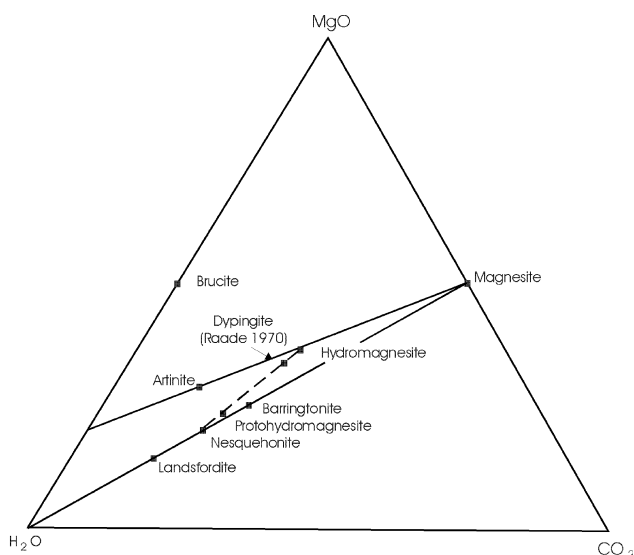
Figure 1. Triangular plot of compositional characteristics of common magnesium hydrates and hydroxyl carbonates (from Davies and Bubela 1973). Note that the empirical formula for "light" hydromagnesite shows four water molecules and that "heavy" hydromagnesite has five water molecules (e.g., Botha and Strydom 2001), that is, the same chemical composition as stochiometric dypingite: $Mg_5(CO_3)_4(OH)_2 \cdot 5H_2O$. Note that the magnesium pentahydrate carbonate, landsfordite, precipitates from magnesium bicarbonate solutions at temperatures below 13°C. The pseudomorphic replacement of landsfordite by nesquehonite at room temperature is spontaneous and irreversible (Hill et al. 1982).

some calcium. The nucleation and growth rate of $CaCO_3$ is strongly affected by the presence of Mg^{2+}, while lattice strain due to the incorporation of magnesium ions increases the solubility of calcite (e.g., Aikin and Lagerwerff 1965; Folk 1974; Berner 1975; Reddy and Wang 1980; Mucci and Morse 1983; Compton and Brown 1994; Pokrovsky 1998; Chen et al. 2006). The quantity of Mg^{2+} incorporated into the calcite is also affected by the precipitation rate (e.g., Garrels and Wollast 1978). High magnesium concentrations in aqueous solutions can also potentially inhibit calcite formation, preferentially allowing monohydrocalcite or aragonite to precipitate (Lippmann 1973).

When thermally unstable nesquehonite exists in an aqueous system close to supersaturation with $CaCO_3$, the rise in pH promoted by nesquehonite dissolution can potentially promote calcite precipitation, the ensuing fall in pH accelerating continued nesquehonite dissolution (Davies et al. 1977). This means that the progress of the nesquehonite-hydromagnesite transformation (N→HM) may be influenced by calcium carbonate dissolution-

precipitation kinetics and that, conversely, the progress of the N→HM transition may influence calcium carbonate mineralogy and mineral chemistry. Here we report an experiment devised to evaluate the nature of the material products of the N→HM transition in the system CaO-MgO-H_2O-CO_2.

Material and Methods

Experimental Procedure. Pulverized $Mg(OH)_2$ (2.90 g, 0.05 mol) and $CaCl_2 \cdot 2H_2O$ (1.47 g, 0.01 mol) were suspended in water (150 mL). The suspension was stirred at room temperature ($Mg^{2+}_{(aq)}/Ca^{2+}_{(aq)} = 5:1$), and CO_2 was bubbled through it for 12 h at 25°C. During this period, the pH dropped from 10.5 to 6.6. The addition of CO_2 was continued until the slurry pH stabilized. At this point the CO_2 flow was stopped. The suspension was filtered and the residue allowed to dry in air. The vibrational spectrum was measured. The residue was resuspended in the filtrate and heated at 35°C for 12 h. After filtration and air drying, the vibrational spectrum was remeasured. This procedure was continued, heating at 44°C, with the experimental cell covered to prevent reequilibration of the system with atmospheric CO_2. Precipitates in association with the mother liquor were held at 52°C for 336 h and then at 60°C for a further 192 h. At 52° and 60°C a continuous crust of precipitated crystals (surface film) formed at the interface between the mother liquor and the atmosphere, in addition to precipitates lining the floor of the experimental vessel (substrate). Accordingly, analyses were undertaken for both substrate and film precipitates.

Analytical Methods. Identification of minerals was performed on powders of the synthesized precipitates. All powders were lightly ground and air dried at 25°C for 24 h. Techniques employed were Fourier-transform mid-infrared (FT-IR), FT-Raman, and x-ray diffraction (XRD). All analyses were conducted at 25°C. Raman analyses were undertaken (with a 1064-nm NdYAG laser source) in the range 150–2000 cm^{-1} using a Nicolet Nexus FT-Raman module. Sharp bands are probably accurate to within 2 cm^{-1}. Infrared analyses were performed in the range 600–4000 cm^{-1} using a Nicolet Avatar 320 FT-IR spectrometer fitted with a diamond attenuated total reflectance accessory. Electron microscopic analyses were conducted with a Jeol JSM6310 scanning electron microscope (SEM) with an Oxford Instruments ISIS energy dispersive spectrometer. FT-Raman, FT-IR, and SEM analyses were conducted at the University of Brighton. The

pH measurements were undertaken at 25°C with a Mettler Toledo MP220 meter. The readings are accurate to 0.01 pH.

The XRD analyses were undertaken with a position-sensitive detector (PSD) at the Natural History Museum, London. X-ray powder diffraction data were collected using a Nonius PDS120 Powder Diffraction System with an INEL curved PSD. This detector has an output array of 4096 digital channels representing an arc of 120° 2θ and permits the simultaneous measurement of diffracted x-ray intensities at all angles of 2θ across 120° with a static beam-sample-detector geometry. Copper K_1 radiation was selected from the primary beam using a germanium (111) single-crystal monochromator, and horizontal and vertical slits were used to restrict the beam to 0.24×5.0 mm. For these samples, measurements were made in reflection geometry with the powder sample surface at a fixed angle of 10° to the incident beam, to ensure good peak resolution. Data collection times were 40 min for each sample. The angular range recorded was 10°–120° 2θ. National Institute of Standards silicon powder SRM640, silver behenate, and Y_2O_3 were used as external 2θ calibration standards, and the 2θ linearization of the detector was performed using a least squares cubic spline function.

Raman Spectroscopic Study of Calcium and Magnesium Carbonates

The Raman spectroscopic signatures of magnesium and calcium carbonates are found in three wavenumber regions: 1500–1000, 1000–500, and 500–100 cm^{-1} (e.g., Scheetz and White 1977; Edwards et al. 2005a). In general, bands at frequencies above 500 cm^{-1} are due to the internal motions of the molecular carbonate ion (internal modes), and those below 500 cm^{-1} are due to motions involving the entire lattice cell (lattice modes). Within the 1500–1000-cm^{-1} region, the symmetrical stretching mode v_1 of the CO_3^{2-} ion is the strongest band observed in the Raman spectrum of the carbonates. The antisymmetric stretching v_3 Raman band of CO_3^{2-} is of lower intensity than v_1 but usually occurs near 1400 cm^{-1}. The antisymmetric bending vibration v_4 occurs near 700 cm^{-1}. Lattice external modes occur in the low-wavenumber region (100–500 cm^{-1}). Because the v_1 Raman stretching wavenumbers are higher for the magnesium carbonates than for their calcium analogues, the v_1 stretching vibration in isolation can be used to differentiate between groups of either calcium or magnesium carbonates. However, the v_1 mode in isolation is not sufficient for the unequivocal identification of individual calcium or magnesium car-
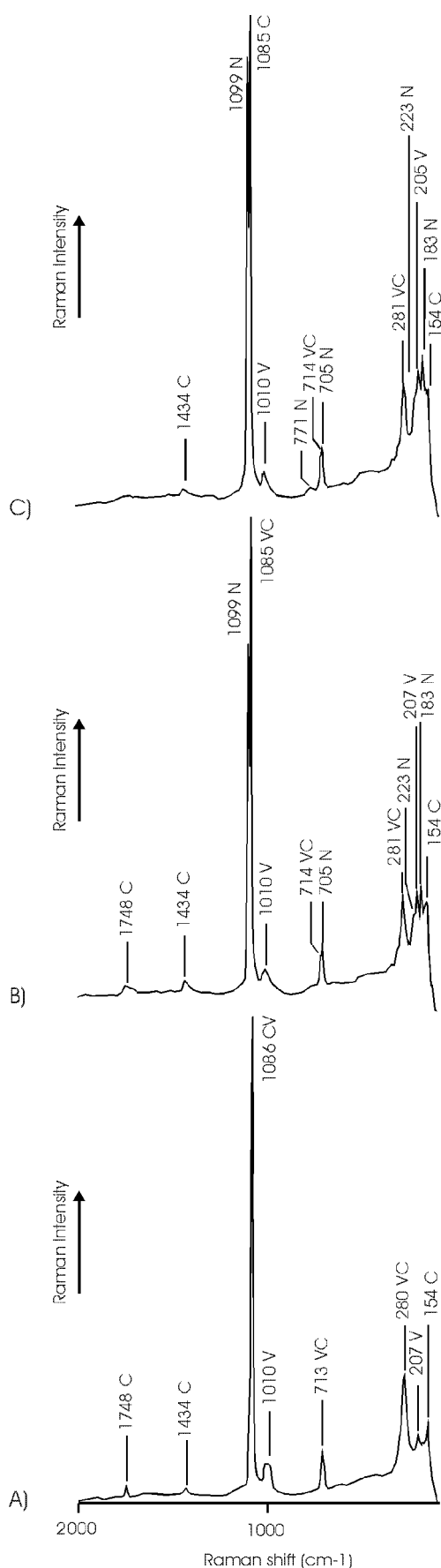
bonates in each group (Edwards et al. 2005a). Identification of mineral phases in mixed calcium-magnesium carbonate assemblages requires corroboration with other characteristic bands and, where appropriate, employment of complementary analytical techniques.

Experimental Results

Synthesized Precipitates, 25°–44°C (12 h).   The Raman spectrum of the precipitates formed as the pH dropped from 10.5 to 6.6 with CO_2 addition at 25°C is presented in fig. 2A. The three polymorphs of $CaCO_3$ (aragonite, calcite, and vaterite) show strong overlap in the 1085–1088-cm^{-1} region. Moreover, the v_1 mode of calcite, together with various other internal and lattice modes, range in frequency and band width as a function of $MgCO_3$ content (Bischoff et al. 1985). The presence of a band centred at ~1010 cm^{-1} (a prototypical feature of vaterite), together with several lattice vibrations that can be assigned to calcite and/or vaterite, indicates a mixture of the two polymorphs. Vaterite is frequently formed in laboratory settings when $CaCO_3$ is precipitated rapidly. The polymorph is unstable with respect to calcite and can rapidly transform to the stable polymorph calcite through dissolution-precipitation reactions, the Mg^{2+} ion accelerating the crystal transformation process (Chen et al. 2006; Han et al. 2006).

The absence of resolvable bands at 1904, 1574, 1462, and 704 cm^{-1} and of several lattice modes associated with aragonite suggests that the polymorph is not present, at least in any great abundance. Aragonite is frequently reported to form instead of calcite in magnesium-rich aqueous solutions (e.g., Lippmann 1973). The apparent absence of the polymorph may result from the low temperature of calcium carbonate precipitation (e.g., Han et al. 2006). Further, synthetic magnesian calcites in the <15-mol% range show products with ion activity lower than that of the equilibrium solubility product of aragonite (Bischoff et al. 1987).

The Raman spectrum of the precipitates formed after the residue was resuspended in the filtrate and heated at 35°C shows Raman-active bands for calcite and vaterite. Also present is a high-intensity band at 1099 cm^{-1}, which together with bands at 187, 228, and 703 cm^{-1} indicate the presence of nesquehonite (fig. 2B). The pH of the 35°C mother liquor was measured at 7.08. The intensity of the 1099-cm^{-1} v_1 band of nesquehonite relative to background increases between 35° and 44°C (fig. 2C), with a discontinuous film of acicular nesquehonite crystals apparent at the surface of the mother liquor by 44°C. The pH of the solution
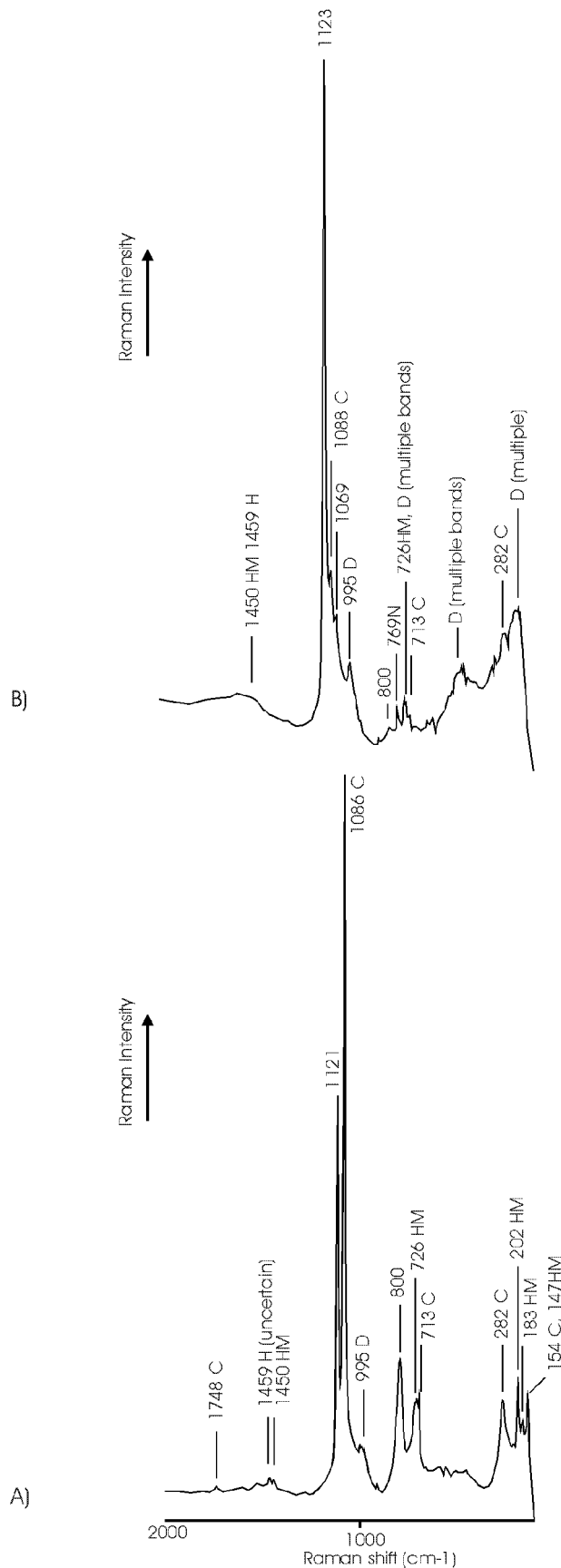
Figure 2. Raman spectra of 25°C (12 h; *A*), 35°C (12 h; *B*), and 44°C (12 h; *C*) precipitates. *C* = calcite, *N* = nesquehonite, and *V* = vaterite.

was 7.45 close to the surface of the mother liquor, compared to 7.33 close to the calcite-bearing substrate, consistent with progressive CO_2 degassing of the mother liquor.

Synthesized Precipitates, 52°C (336 h), FT-Raman Analysis. At the transition temperature, the surface film of precipitates was sufficiently developed for sampling. The pH of the mother liquor was measured at 7.50 directly below the surface film and at 7.53 just above the substrate. The Raman spectrum of the substrate shows that calcite is the dominant phase (fig. 3*A*). A subordinate band at 1121 cm^{-1} is broadly coincident with the v_1 internal mode of the unidentified amorphous compound (UIC) of Lanas and Alvarez (2004). This mineraloid was produced over short experimental durations during heating of dried nesquehonite at >115°C. The 1121-cm^{-1} band is also broadly coincident with the v_1 band of hydromagnesite, which has been reported at frequencies ranging from 1117 to 1120 cm^{-1} (e.g., White 1974; Edwards et al. 2005*a*), and huntite, reported at 1123 cm^{-1} (Scheetz and White 1977).

Various lattice bands in the spectrum can be assigned to calcite, hydromagnesite, and dypingite. An additional medium-intensity band centered at ~800 cm^{-1} is present. This band is barely resolvable in the surface film spectrum (fig. 3*B*). The 800-cm^{-1} band is coincident with the infrared-active Raman-forbidden v_2 carbonate bending vibration of hydromagnesite and occurs in conjunction with Raman-active hydromagnesite bands at 183, 202, 726, and 1450 cm^{-1} (fig. 3*A*). To clarify the nature of the Raman-active 800-cm^{-1} band, a subsample of the substrate was held in the presence of the mother liquor for an additional 168 h at 52°C (for a total of 504 h). The Raman spectrum shows a dramatic increase in the intensity of the 800-cm^{-1} band relative to the substrate at 336 h. The intensity of the 800-cm^{-1} band exactly equals that of the 1121-cm^{-1} band. The v_1 calcite band is subordinate in intensity. The Raman-active hydromagnesite bands, particularly the 726-cm^{-1} band, are higher in intensity than those from the 336-h experiment. The evident growth of the 800-cm^{-1} band at the N→HM transition and its coincidence with the infrared-active Raman-forbidden carbonate bending band of hydromagnesite suggest a relaxation of

Figure 3. Raman spectra of 52°C (336 h) (*A*) substrate and (*B*) surface film. *C* = calcite, *D* = dypingite, *H* = huntite, *HM* = hydromagnesite, and *N* = nesquehonite. The likely sources of unassigned peaks are discussed in "Synthesized Precipitates, 52°C (336 h), FT-Raman Analysis".

selection rules, which can occur when distorted crystal structures are generated by rapid precipitation (e.g., White 1974). Rapid synthesis of crystals at low temperatures means that mineral structures frequently do not reequilibrate readily into a well-ordered form (e.g., Scheetz and White 1977).

The Raman spectrum of the 336-h surface film shows a high-intensity band coincident with the intense v_1 vibration mode of huntite and broadly coincident with the v_1 band of hydromagnesite and the UIC (fig. 3*B*). No other bands could be assigned to huntite. However, it is interesting to note that the resolution of Raman-active bands from natural samples of huntite is variable and includes samples in which the v_1 mode is the only resolvable band (Scheetz and White 1977). Three low-intensity shoulders on the 1123-cm^{-1} band are assigned to calcite, monohydrocalcite (tentatively), and dypingite. Low-intensity bands at 769 cm^{-1} and just over 1500 cm^{-1} suggest residual traces of nesquehonite. Barely resolvable bands at 800 and 726 cm^{-1} suggest traces of hydromagnesite in the surface film, although it is evident that hydromagnesite precipitation is less advanced than in the associated 336-h substrate, in which Raman-active lattice modes of hydromagnesite are clearly resolved alongside the Raman-forbidden v_2 mode of hydromagnesite. Accordingly, XRD and FT-IR analyses were performed on the surface film to further characterize the nature of the transitory phase(s) present immediately before the onset of widespread hydromagnesite precipitation.

Surface Film Precipitates, 52°C (336 h), XRD Analysis. The diffraction pattern indicates the presence of nesquehonite, dypingite, and huntite (fig. 4). However, peaks at $d = 22.28$ and 11.14 Å indicate that the main phase present is not a recognized magnesium hydroxyl or hydrate carbonate but probably has a layered structure, because its low-angle reflections can be indexed as first and second order, that is, 001 and 002, with $d(001) = 22.28$ Å. These peaks are not apparent in the XRD analysis of "protohydromagnesite" presented by Davies and Bubela (1973). Protohydromagnesite (for which no vibrational spectra have been published) is extensively similar in chemical composition to barring-
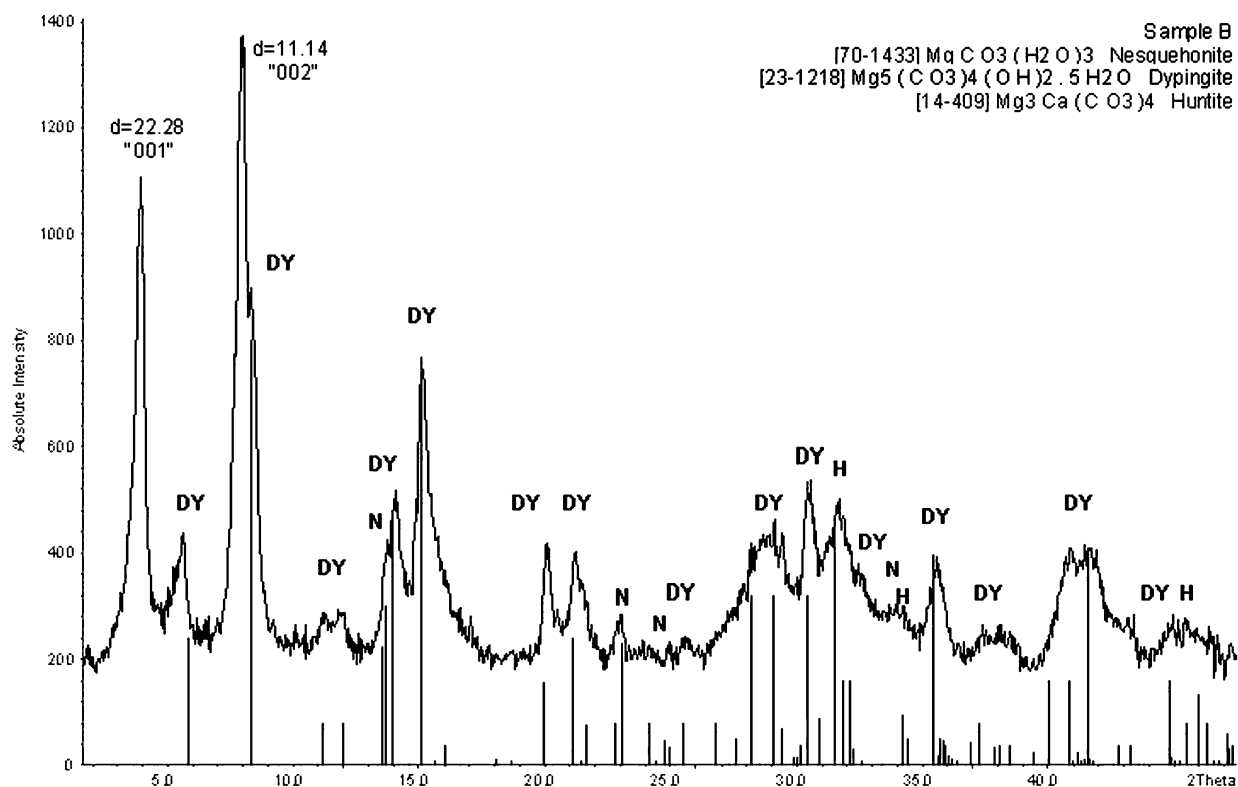
Figure 4. X-ray diffraction pattern of the 52°C (336 h) surface film precipitates.

tonite (fig. 1). In our work, XRD indicates the existence of an N→HM transitory mineral phase in addition to dypingite and protohydromagnesite.

Surface Film Precipitates, 52°C (336 h) FT-IR Analysis. The spectrum presented in fig. 5 shows that various bands that can be assigned to dypingite and/ or hydromagnesite. It has previously been suggested that dypingite may be a transitory phase in the N→HM transformation (Davies and Bubela 1973). Sharp bands at 1420 and 1476 cm^{-1} are consistent with the CO$_3^{2-}$ v_3 stretching vibrations of both minerals and rule out the presence of the UIC. The spectrum also shows a broad band at ~1000 cm^{-1}, consistent with dypingite (Raade 1970). However, the strong absorption band at 3650 cm^{-1}, which results from OH$^-$ groups in hydromagnesite and dypingite, is not resolved. Further, strong absorption at 1645 cm^{-1} (e.g., Raade 1970; White 1974; Lanas and Alvarez 2004) and the absence of a clearly resolved CO$_3^{2-}$ bending band at 800 cm^{-1} are inconsistent with hydromagnesite and/or dypingite being the dominant constituents of the surface film. Hence, although the spectrum is composite in nature (because of the multimineral makeup of the surface film), FT-IR suggests that the layered main phase reported by XRD is a previously uniden-

tified transitory magnesium hydrate carbonate (TMHC).

Extensive overlap exists between the infrared spectra of huntite and those of magnesium hydroxyl
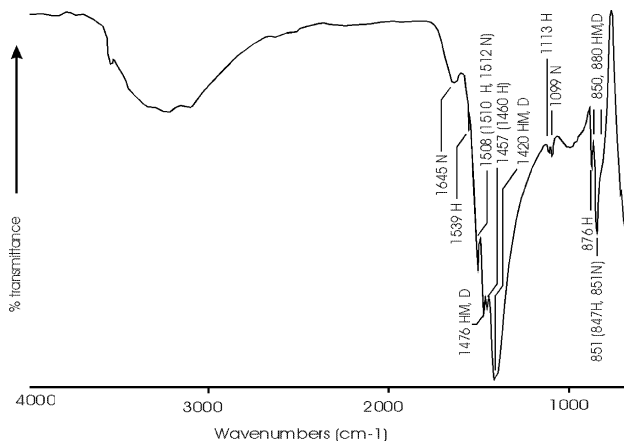

Figure 5. FT-IR spectrum of the 52°C (336 h) surface film. C = calcite, D = dypingite, H = huntite, HM = hydromagnesite, and N = nesquehonite. The likely sources of unassigned peaks are discussed in "Surface Film Precipitates, 52°C (336 h) FT-IR Analysis."

and hydrate carbonates (e.g., Raade 1970; White 1974). Further, variability exists in the reported numbers and assigned frequencies of huntite infrared-active bands (e.g., Scheetz and White 1977; Kangal et al. 2005). The mid-infrared spectrum of the surface film shows a couplet of bands located at 851 cm^{-1} and a shoulder at 877 cm^{-1}. The frequencies closely correspond to the huntite v_2 bands reported, in two different studies, at 847 and 877 cm^{-1} (Böttcher et al. 1997) and 858 and 880 cm^{-1} (Scheetz and White 1977). Also present is a band at 1113 cm^{-1}, broadly coincident with the huntite infrared-active v_1 band variously reported at 1110, 1113, and 1105 cm^{-1} (Scheetz and White 1977; Böttcher et al. 1997). Several mid-infrared-active bands for huntite associated with splitting of v_3 have been cited in the region 1450–1430 cm^{-1}. Bands at 1539, 1508, and 1457 cm^{-1} (fig. 5) correspond to reported bands at 1535, 1510, and 1460 cm^{-1} (Scheetz and White 1977).

Synthesized Precipitates, 336 h at 52°C and 192 h at 60°C. The Raman spectra of the substrate and surface film both show a high-intensity band at 1121 cm^{-1} that, with several weaker bands, is assigned to hydromagnesite (fig. 6). A subordinate band at 995 cm^{-1} is assigned to dypingite. The intensity of this band in the substrate and film is far greater than that recorded at 52°C. No 800-cm^{-1} band is unambiguously resolved in either spectrum. The presence of a shoulder at 1069 cm^{-1} in both spectra may suggest the presence of traces of mono-hydrocalcite.

The FT-IR spectrum of the surface film shows an absorption band resulting from OH^- groups at 3650 cm^{-1} and the CO_3^{2-} bending band at 800 cm^{-1} (fig. 7). Various other bands can similarly be assigned to dypingite and/or hydromagnesite. UIC is not detected. Huntite is not clearly resolved in the spectrum. However, line overlap of huntite with hydromagnesite and dypingite is extensive, and the relative strength of absorption bands at 850 and 880 cm^{-1}, together with strong absorption at 1115 cm^{-1}, suggests that huntite may be present.

SEM Analysis. The 52°C (336 h) surface film is characterized by abundant platy aggregates of magnesium carbonates (fig. 8A). The aggregates are texturally distinct from accounts of natural occurring dypingite or barringtonite but are texturally similar to synthesized protohydromagnesite and some natural and synthesized hydromagnesite. However, it should be noted that radiating globular aggregates of natural dypingite may result from transformation of nesquehonite in the dry state. In addition, the dry-state N→HM transformation occurs without apparent change in crystal morphology (Dell and Weller 1959; Davies and Bubela 1973).
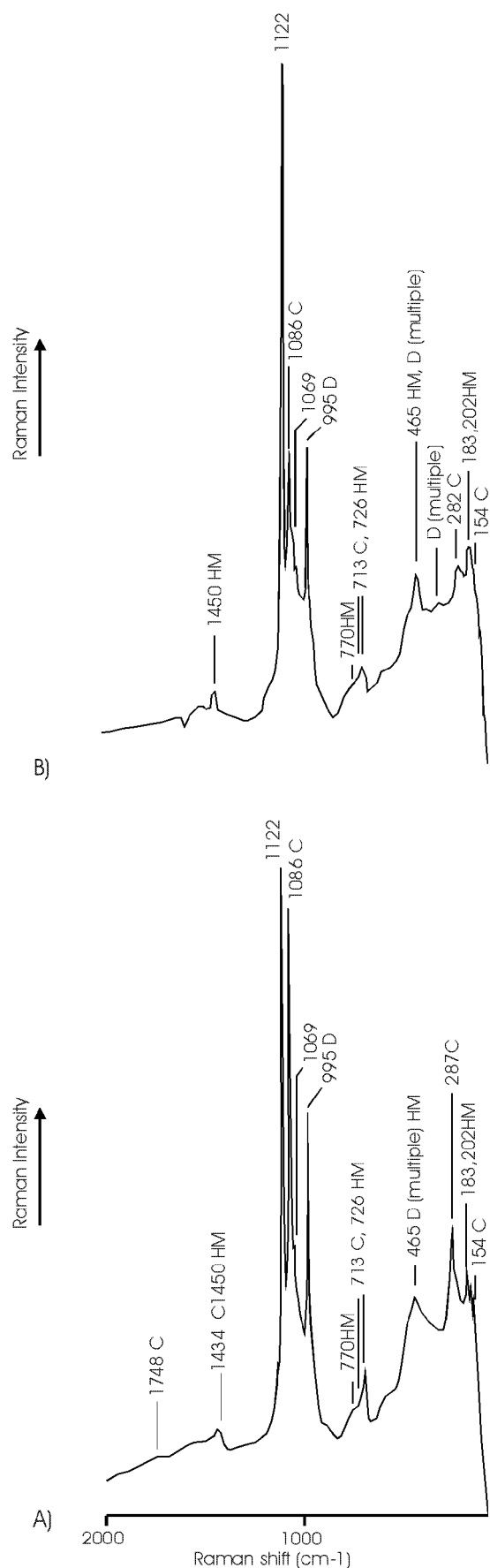
Huntite crystals occur with platy rhomboidal habits, aggregated into compact masses a few microns in diameter and hosted by the platy magnesium hydrate carbonates (fig. 8B). The textural occurrence and size ranges of the crystals are comparable to those of natural huntite (e.g., Dollase and Reeder 1986). Also present in the surface film are small quantities of acicular magnesium carbonates (fig. 8C). They are texturally comparable to nesquehonite synthesized in the early stages of the experiments and to synthesized nesquehonite in previous reports (e.g., Davies and Bubela 1973).

Nesquehonite aggregates host small rounded or dumbbell-shaped magnesium-bearing calcite crystals. The surfaces of the crystals are pitted and irregular (fig. 8D). The Mg^{2+} ion is known to influence calcite crystal morphology: the ion adsorbs on the surface of calcite, causing an increase in surface roughness and distortion of crystals (Chen et al. 2006). Analysis of the substrate revealed the same textural variability. All calcite crystals inspected were magnesium bearing. The magnesian calcite crystals range in size from a few microns up to ~100 µm and show variable $MgCO_3$ content. Magnesian calcites with up to 20 mol% $MgCO_3$ content have been reported from a number of low-temperature natural and experimental environments (e.g., Lippmann 1973; Bischoff et al. 1987).

The 60°C surface film contains platy aggregates of magnesium carbonate texturally comparable to natural and some synthesized hydromagnesite (documented in, e.g., fig. 8E). The surfaces of the magnesium hydroxyl carbonates are variably overgrown with huntite (fig. 8F). No textures comparable to nesquehonite were detected, although rare magnesium-bearing calcite crystals showing morphologies extensively similar to those of the 52°C surface film precipitates were detected. Analysis of the substrate revealed the same textural variability with abundant magnesian calcite. No well-developed rhombohedral calcite crystals were encountered. Generally high $Mg^{2+}_{(aq)}/Ca^{2+}_{(aq)}$ activity in pore waters accounts for calcite crystal morphologies and the low total numbers of calcite in the surface films, because increasing the $Mg^{2+}_{(aq)}/Ca^{2+}_{(aq)}$ ratio in the mother liquor can promote a decrease in abundance of $CaCO_3$ crystals (Chen et al. 2006).
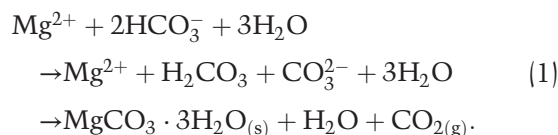
Discussion

Nesquehonite Formation. Presented in figure 9, plotted against temperature, are the pH readings and intensities of the v_1 bands of calcite, nesque-

honite, and dypingite (measured as a ratio relative to background), along with those of the band situated approximately equidistant between the v_1 bands of huntite, hydromagnesite, and most likely TMHC (variably recorded between 1120 and 1123 cm^{-1}). The majority of $CaCO_3$ was precipitated as substrate at 25°C. A reduction at 35°C coincides with the appearance of nesquehonite and an increase in pH (fig. 9). A decrease in pH at 44°C is coincident with an increase in the intensity of the v_1 band of calcite and continued increase in the intensity of the v_1 mode of nesquehonite. At this stage, a surface tension–mediated discontinuous film of acicular nesquehonite crystals developed at the surface of the mother liquor, conditions being tangibly more acidic in the static pore waters close to the magnesian calcite enriched substrate.

Experimental results link nesquehonite formation to the decrease in solubility of CO_2 gas in water with increasing temperature (e.g., Pierantozzi 1993; Botha and Strydom 2001). Magnesium bicarbonate solutions deposit nesquehonite depending on the concentration on dissolved carbon dioxide: at concentrations of 2–19 g dm^{-2} at 20°C, nesquehonite forms; at lower concentrations, 0.27–2 g dm^{-2}, artinite forms (Kazakov et al. 1959). The formation of nesquehonite during $CO_{2(aq)}$ degassing takes place in two steps (Menzel and Brückner 1930). Implicit in this is that the escape of carbon dioxide leads to the continued hydrolysis of the bicarbonate ion into carbonate (e.g., Deelman 2005):

$$Mg^{2+} + 2HCO_3^- + 3H_2O$$
$$\rightarrow Mg^{2+} + H_2CO_3 + CO_3^{2-} + 3H_2O \qquad (1)$$
$$\rightarrow MgCO_3 \cdot 3H_2O_{(s)} + H_2O + CO_{2(g)}.$$

The Nesquehonite → Hydromagnesite Transition. At temperatures greater than 50°C, nesquehonite readily converts to hydromagnesite (e.g., Davis and Bubela 1973). The decomposition of nesquehonite in an aqueous medium involves hydroxyl formation and the continuous addition of dissolved carbon dioxide to the mother liquor, with transitory


Figure 6. Raman spectra of 60°C precipitates substrate (A) and surface film (B). C = calcite, D = dypingite, H = huntite, and HM = hydromagnesite. The likely sources of unassigned peaks are discussed in "Synthesized Precipitates, 336 h at 52°C and 192 h at 60°C."
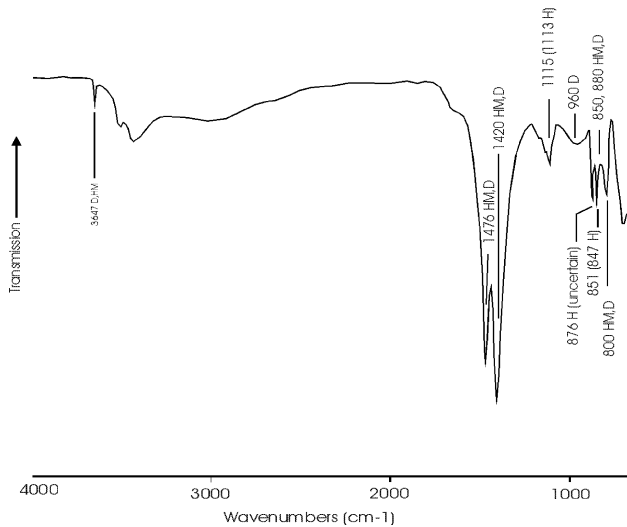
Figure 7. FT-IR spectrum of the 60°C surface film. The infrared spectra of dypingite and hydromagnesite are extensively similar (Raade 1970; White 1974). Absorption bands resulting from OH^- groups (3650 cm^{-1}) and water of crystallization (3510 and 3450 cm^{-1}) are identical for both, as are CO_3^{2-} stretching bands (1480, 1420, and 1120 cm^{-1}) and CO_3^{2-} bending bands (880 and 850 cm^{-1}).
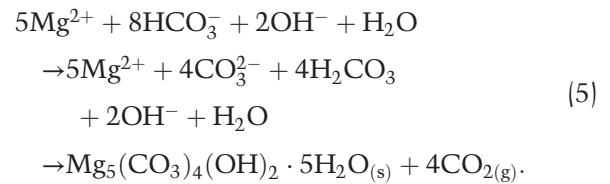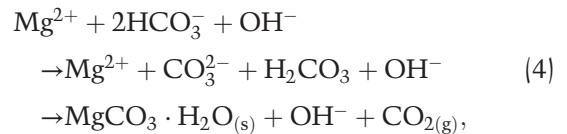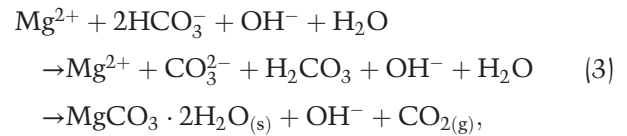
phase(s) forming over a narrow thermal interval from the dissociation products (Davies et al. 1977):

$$MgCO_3 \cdot 3H_2O_{(s)} + H_2O$$
$$\rightarrow Mg^{2+} + HCO_3^- + OH^- + 2H_2O. \tag{2}$$
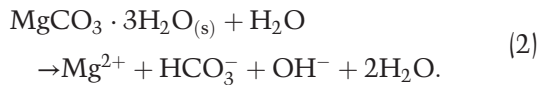
The simplest approximation of the chemical formula for protohydromagnesite is $MgCO_3 \cdot 2H_2O$. Its growth at the expense of nesquehonite represents water loss (Davies and Bubela 1973). The time frame for production of TMHC was double that for protohydromagnesite, and therefore TMHC most likely represents water loss relative to the dihydrate. Accordingly, TMHC may approximate to a monohydrate. Although magnesium monohydrate carbonate has not yet been found in nature, it has been synthesized during the dry thermal decomposition of nesquehonite (e.g., Menzel and Brückner 1930; Dell and Weller 1959) and may be an extremely short-lived transitory phase during the N→HM transition in an aqueous medium.

At the transition temperature, CO_2 addition to the mother liquor would be ongoing, as a consequence of dissolution of metastable carbonate phases and the effect of temperature on the solubility of CO_2 in water. Accordingly, transitory magnesium hydrate and hydroxyl carbonates may

have formed consecutively in a sequence of dewatering dissolution-precipitation steps, accompanying $CO_{2(aq)}$ degassing. The proportionality of CO_2 fixed in mineral phases, relative to CO_2 gas escape, is not known, but it may approximate the following equations:

$$Mg^{2+} + 2HCO_3^- + OH^- + H_2O$$
$$\rightarrow Mg^{2+} + CO_3^{2-} + H_2CO_3 + OH^- + H_2O \tag{3}$$
$$\rightarrow MgCO_3 \cdot 2H_2O_{(s)} + OH^- + CO_{2(g)},$$

$$Mg^{2+} + 2HCO_3^- + OH^-$$
$$\rightarrow Mg^{2+} + CO_3^{2-} + H_2CO_3 + OH^- \tag{4}$$
$$\rightarrow MgCO_3 \cdot H_2O_{(s)} + OH^- + CO_{2(g)},$$

$$5Mg^{2+} + 8HCO_3^- + 2OH^- + H_2O$$
$$\rightarrow 5Mg^{2+} + 4CO_3^{2-} + 4H_2CO_3$$
$$+ 2OH^- + H_2O \tag{5}$$
$$\rightarrow Mg_5(CO_3)_4(OH)_2 \cdot 5H_2O_{(s)} + 4CO_{2(g)}.$$

The Behavior of Magnesian Calcite. Reactions (1)–(5) indicate the transient production of HCO_3^-. The apparent decline in the solution pH with calcite precipitation at 44°C implies temporal availability of HCO_3^- to react with $Ca_{(aq)}^{2+}$ to form calcite, thereby depressing the pH by $H_{(aq)}^+$ liberation (e.g., Jiménez-López et al. 2001). Transient increases in H^+ also leads to an increase in $CO_{2(aq)}$ in solution, with the CO_2 either gradually escaping or being fixed in precipitating phases. It also follows that acceleration of nesquehonite dissolution by calcite formation may be limited by the progressive rise in $Mg_{(aq)}^{2+}/Ca_{(aq)}^{2+}$ gradually inhibiting calcite precipitation.

The thermodynamic stability of magnesian calcites has been the subject of many studies (e.g., Bischoff et al. 1987; Königsberger and Gamsjäger 1992). Dissolution congruency may vary with time and composition and may lead to the precipitation of secondary low-magnesium calcites and Mg^{2+} enrichment in pore solutions (e.g., Bischoff et al. 1987; Busenberg and Plummer 1989). Hence, thermally driven dissolution of magnesian calcite would most likely impart isothermal temporal heterogeneity in pore solution chemistries. Further, compositional limitation of high-magnesium calcites may be caused by the formation of the more stable compound huntite, formation of the latter potentially preventing the formation or causing
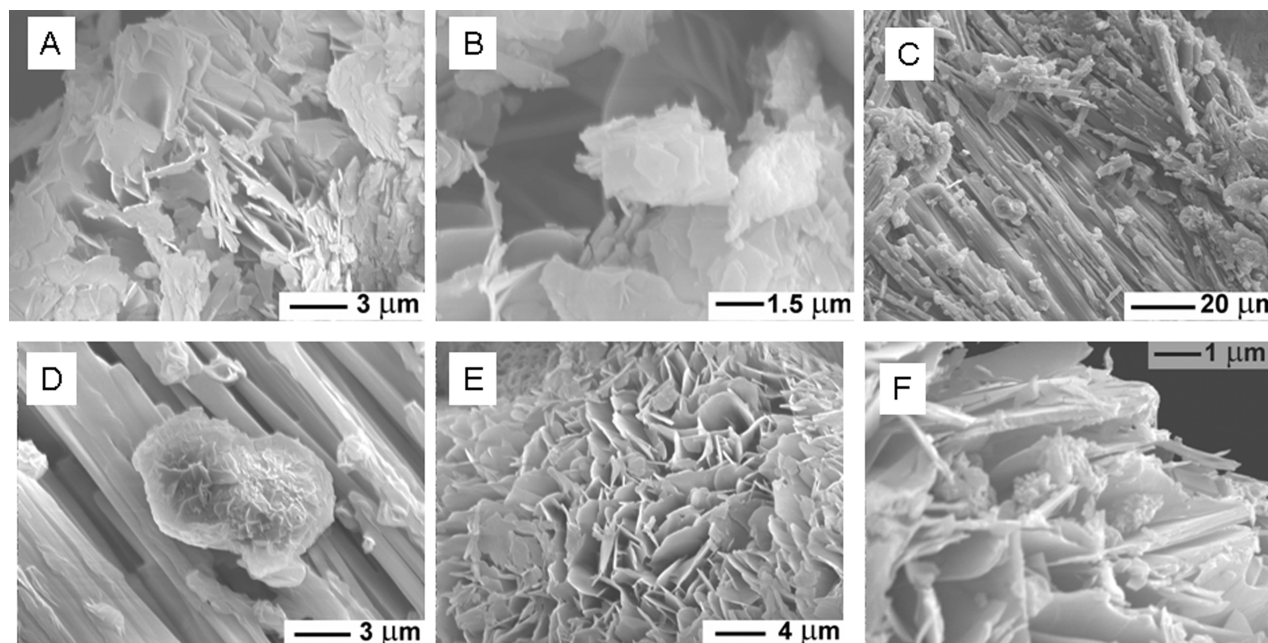
Figure 8. Back-scattered scanning electron microscope images of experimental precipitates. *A*, 52°C (336 h) surface film precipitates: platy magnesium carbonates texturally comparable to previous documented accounts of hydromagnesite and protohydromagnesite (Davis and Bubela 1973). *B*, 52°C (336 h) surface film precipitates: platy rhomboidal aggregates of huntite. The textural occurrence of huntite is as late-stage primary precipitates, associated with transitory magnesium hydrate and/or hydroxyl carbonate phases. Given that x-ray diffraction, Raman and Fourier transform mid-infrared (FT-IR) analyses indicate the presence of huntite and that there are no reports of calcium substitution in the structure of protohydromagnesite or hydromagnesite (e.g., Davies and Bubela 1973; Queralt et al. 1997), the correspondence of Ca, C, and Mg with the compact masses and the restriction of Ca to these masses identify them as huntite. *C*, 52°C (336 h) surface film precipitates: acicular aggregates of magnesian carbonate (nesquehonite) hosting rounded or dumbbell-shaped magnesian calcite. *D*, 52°C (336 h) surface film precipitates: subspherical magnesian calcite crystal, showing pitted and irregular crystal surface. *E*, 60°C (528 h) surface film precipitates: abundant platy magnesium carbonates. Raman and FT-IR analyses identify this phase as hydromagnesite and/or dypingite. *F*, 60°C (528 h) surface film precipitates: late-stage primary precipitates of huntite overgrowing the surfaces of magnesium hydroxyl carbonates.

the decomposition of higher magnesian calcites (Königsberger and Gamsjäger 1992).

The preferential development of monohydrocalcite over calcite in magnesium-rich aqueous solutions has been documented (e.g., Hull and Turnball 1973; Lippmann 1973). Evidently, its formation in the experiments documented here was occasionally kinetically favored with respect to calcite during the N→HM transition, presumably because of the lower activation energy for its formation with respect to calcite (Jiménez-López et al. 2001) and varying but generally high prevailing $Mg^{2+}_{(aq)}$/ $Ca^{2+}_{(aq)}$. The presence of monohydrocalcite could indicate that its nucleation rate was faster than calcium dehydration kinetics. Alternately, if the $(CaHCO_3)^+$ ion pair was the main Ca-bearing complex in solution during induction and growth of monohydrocalcite (e.g., Jiménez-López et al. 2001), then interaction with increasingly abundant OH^-

groups, afforded by the N→HM transformation process to form $CaCO_3 \cdot H_2O$ (e.g., Stipp 1999; Jiménez-López et al. 2001), may account for its presence. In either event, monohydrocalcite is metastable with respect to calcite (Hull and Turnball 1973) and transforms to the latter through a sequence of dissolution-precipitation reactions (Jiménez-López et al. 2001). Further, dissolution of monohydrocalcite where surrounded by unstable magnesium hydrate carbonates provides a source of calcium for huntite (Davies et al. 1977) and, potentially, elevated $Mg^{2+}_{(aq)}$/$Ca^{2+}_{(aq)}$ ratios to suppress or cause the decomposition of higher magnesian calcite.

Huntite Formation. Huntite forms either by direct precipitation from aqueous solutions or as a result of interaction of such solutions with preexisting carbonates (Kinsman 1967; Dollase and Reeder 1986; Zachmann 1989; Calvo et al. 1995).
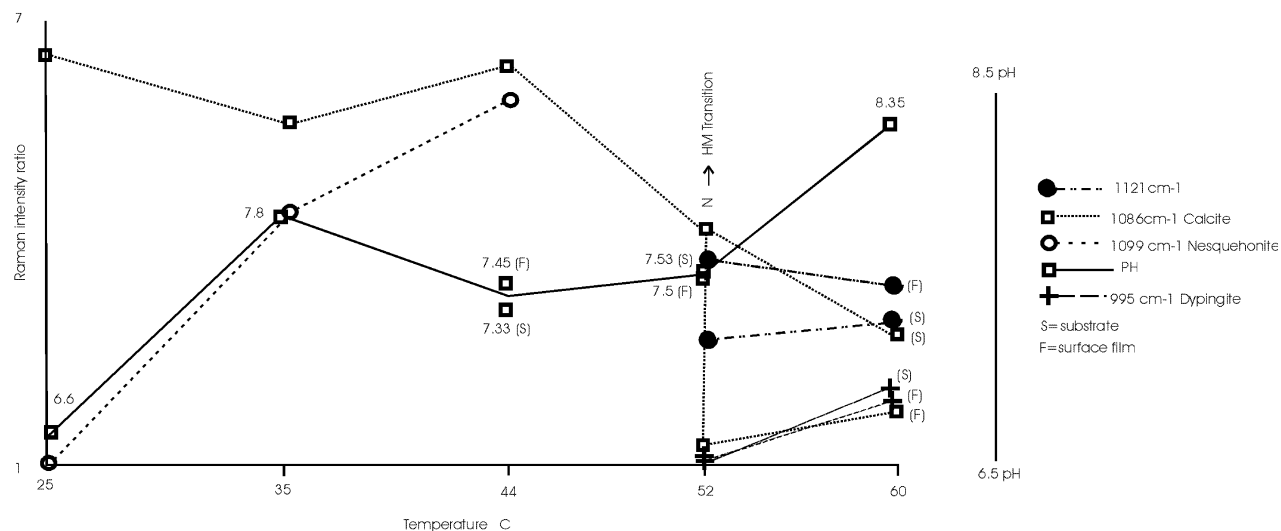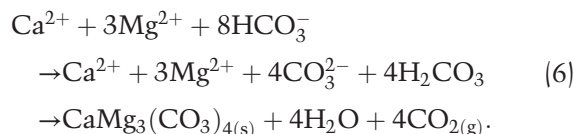
Figure 9. Schematic diagram showing the intensity ratios of the v_1 vibrations of nesquehonite, dypingite, and calcite relative to background measured at 2000 cm^{-1} plotted against temperature. Also plotted is the relative intensity of the band situated approximately equidistant between the v_1 vibration of huntite and hydromagnesite ($\sim$1120 cm^{-1}).

The mineral is scarce in the natural environment and the geological record. To some extent, this is because conditions for its formation may not be common (Walling et al. 1995). However, the mineral is frequently associated with destructive degradation cycles and where occurring in modern sediments is probably subject to progressive replacement during later diagenesis by an equilibrium assemblage such as magnesite-dolomite or dolomite-calcite (Kinsman 1967; Lippmann 1973; Stamatakis 1995). Attempts to measure the solubility of huntite have proven problematic. The reported range of Gibbs energies of formation correspond to a variation of about 7.4 orders of magnitude in the equilibrium solubility product at 25°C (Walling et al. 1995). Further, magnesian huntite with Mg^{2+}/Ca^{2+} ratios as high as 4 have been reported (Stanger and Neal 1994).

In this study, huntite occurs as late-stage primary precipitate, associated with transitory magnesium carbonates. The requisite conditions for huntite formation include a high Mg$^{2+}_{(aq)}$/Ca$^{2+}_{(aq)}$ ratio, high CO$_3^{2-}$ concentrations (e.g., Stanger and Neal 1994; Walling et al. 1995), and a sufficient induction period for nucleation and growth. The conditions were evidently met during the N→HM transition. The textural occurrence of huntite is accounted for by the progressive depression of the Mg$^{2+}_{(aq)}$/Ca$^{2+}_{(aq)}$ ratio with transitory magnesium carbonate formation sourced by the N→HM transitory steps, in a high-CO$_3^{2-}$ environment with Ca$^{2+}_{(aq)}$ derived from monohydrocalcite and magnesian calcite dissolution:

$$Ca^{2+} + 3Mg^{2+} + 8HCO_3^-$$
$$\rightarrow Ca^{2+} + 3Mg^{2+} + 4CO_3^{2-} + 4H_2CO_3 \qquad (6)$$
$$\rightarrow CaMg_3(CO_3)_{4(s)} + 4H_2O + 4CO_{2(g)}.$$

Metastable Mineral Phases and the Ostwald Step Rule. A feature of the 52°C precipitates is the presence of four metastable magnesium carbonates in conjunction with at least three metastable calcium-bearing carbonates. In many low-temperature systems, mineral precipitation follows the Ostwald step rule, in which metastable phases nucleate and are progressively replaced by more stable phases (e.g., Morse and Casey 1988; Deelman 1999; Jiménez-López et al. 2001). However, apparent mineral stabilities are affected by factors such as surface area/solution volume ratio, the solid/solution ratio, particle size, and precipitation of phases within the pore solution network (e.g., Bischoff et al. 1987). The high solids-to-liquid ratios in the experiment documented here also means that pore-scale chemical changes, notably in CO$_{2(gas)}$, HCO$_3^-$, and CO$_3^{2-}$ concentrations, pH, and Mg$^{2+}_{(aq)}$/Ca$^{2+}_{(aq)}$ ratio, would exist. In such a setting, stability of metastable phases may not depend as much on averaged values described in the macroscopic parameters as on local crossings of the supersaturation limit (e.g., Deelman 1999).

Experimental results indicate preferential advancement of the N→HM transition in the magnesian calcite–enriched substrate relative to coexisting surface film. The latter represents the air-solution interface and a porous membrane to escaping CO_2. However, the surface film remained largely saturated at all times, and the evolution of the calcium-bearing carbonate mineralogy at the N→HM transition is common to both film and substrate. Hence, differences in availability of $Ca^{2+}_{(aq)}$ to influence pH through calcite precipitation may account for the apparent disparity in the progress of the N→HM transition. Given this, it follows that pore-scale periodical fluctuations of variable magnitude in pH, dissolved CO_2, and $Mg^{2+}_{(aq)}/Ca^{2+}_{(aq)}$ are attributes of the transformation process, arising in the absence of externally imposed periodic events.

Conclusions

The material products of the N→HM transition are strongly controlled by experiment duration. A hitherto undocumented short-lived TMHC develops immediately before the onset of hydromagnesite precipitation. The TMHC may well grow at the expense of protohydromagnesite. While the complete Raman spectroscopic signature of both minerals remains to be established, the v_1 mode of the TMHC closely coincides with the v_1 modes of huntite and hydromagnesite, producing a complicating factor in interpretation of Raman data. The growth of hydromagnesite at the expense of TMHC is sufficiently rapid for relaxation in Raman selec-

tion rules to occur. The absence of the hydromagnesite v_2 band in the Raman spectra of the 60°C sample implies that subsequent dissolution-crystallization steps strengthen selection rules. The coexistence of dypingite with hydromagnesite indicates that the former mineral is a transitory phase in the N→HM and suggests that pore-scale variability in structural ordering and water content persisted above the transition temperature. The formation of huntite and transitory magnesium hydrate and hydroxyl carbonates can be explained by CO_2 degassing reactions. However, the instability of the transitory phases to transformation also means that huntite may form autonomously in consecutive pulses at the end of each episode of transitory-phase precipitation. Nonuniformity in the progress of the N→HM transition is tied to pore-scale processes, associated variability in aqueous solution chemistries, and local crossings of supersaturation limits. Geochemical feedback between calcium carbonate and transitory phases, through dissolution-precipitation steps, serves to accelerate the N→HM transition.

REFERENCES CITED

Aikin, G. W., and Lagerwerff, J. V. 1965. Calcium carbonate equilibria in solutions open to the air. II. Enhanced solubility of $CaCO_3$ in the presence of Mg^{2+} and SO_4^{2-}. Geochim. Cosmochim. Acta 29: 353–360.

Berner, R. A. 1975. The role of magnesium in the crystal growth of calcite and aragonite from seawater. Geochim. Cosmochim. Acta 39:489–504.

Bischoff, W. D.; Mackenzie, F. T.; and Bishop, F. C. 1987. Stabilities of synthetic magnesian calcites in aqueous solution: comparison with biogenic materials. Geochim. Cosmochim. Acta 51:1413–1423.

Bischoff, W. D.; Sharma, S. K.; and Mackenzie, F. T. 1985. Carbonate ion disorder in synthetic and biogenic magnesian calcites: a Raman spectral study. Am. Mineral. 70:581–589.

Botha, A., and Strydom, C. A. 2001. Preparation of magnesium hydroxyl carbonate from magnesium hydroxide. Hydrometallurgy 62:175–183.

Böttcher, M. E.; Gehlken, P.; and Steele, D. 1997. Characterization of inorganic and biogenic magnesian calcites by Fourier transform infrared spectroscopy. Solid State Ionics 101:1379–1385.

Busenberg, E., and Plummer, L. N. 1989. Thermodynamics of magnesian calcite solid solutions at 25°C and 1 atm total pressure. Geochim. Cosmochim. Acta 53: 1189–1208.

Calvo, J. P.; Stamatakis, M. G.; and Magganas, A. C. 1995. Clastic huntite in upper Neogene formations of the Kozani Basin, Macedonia, northern Greece. J. Sediment. Res. A65:627–632.

Chen, T.; Neville, A.; and Yuan, M. 2006. Influence of

Mg^{2+} on $CaCO_3$ formation: bulk precipitation and surface deposition. Chem. Eng. Sci. 61:5318–5327.

Compton, R. G., and Brown, C. A. 1994. The inhibition of calcite dissolution/precipitation: Mg^{2+} cations. J. Colloid Interface Sci. 165:445–449.

Davies, P. J., and Bubela, B. 1973. The transformation of nesquehonite into hydromagnesite. Chem. Geol. 12:289–300.

Davies, P. J.; Bubela, B.; and Ferguson, J. 1977. Simulation of carbonate diagenetic processes: formation of dolomite, huntite and monohydrocalcite by the reactions between nesquehonite and brine. Chem. Geol. 19:187–214.

Deelman, J. C. 1999. Low-temperature nucleation of magnesite and dolomite. Neues Jahrb. Mineral. Monatsh. 7:289–302.

———. 2005. Low-temperature formation of dolomite and magnesite. Eindhoven, Compact Disc Publications, http://www.jcdeelman.demon.nl/dolomite/bookprospectus.html.

Dell, R. M., and Weller, S. W. 1959. The thermal decomposition of nesquehonite $MgCO_3 \cdot 3H_2O$ and magnesium ammonium carbonate $MgCO_3(NH_4)_2CO_3 \cdot 4H_2O$. Trans. Faraday Soc. 55:2203–2220.

Dollase, W. A., and Reeder, R. J. 1986. Crystal structure refinement of huntite $CaMg_3(CO_3)_4$, with x-ray powder data. Am. Mineral. 71:163–166.

Edwards, H. G. M.; Jorge Villar, S. E.; Jehlicka, J.; and Munshi, T. 2005*a*. FT-Raman spectroscopic study of calcium-rich and magnesium-rich carbonate minerals. Spectrochim. Acta A 61:2273–2280.

Edwards, H. G. M.; Moody, C. D.; Newton, E. M.; Jorge Villar, S. E.; and Russell, M. J. 2005*b*. Raman spectroscopic analysis of cyanobacterial colonization of hydromagnesite, a putative martian extremophile. Icarus 175:372–381.

Folk, R. L. 1974. The natural history of crystalline calcium carbonate: effect of magnesium content and salinity. J. Sediment. Petrol. 44:43–53.

Garrels, R. M., and Wollast, R. 1978. Discussion (Equilibria criteria for two-component solids reacting with fixed composition in an aqueous phase—example: the magnesian calcites). Am. J. Sci. 278:1469–1474.

Han, Y. S.; Hadiko, G.; Fuji, M.; and Takahashi, M. 2006. Factors affecting the phase and morphology of $CaCO_3$ prepared by a bubbling method. J. Eur. Ceram. Soc. 26:843–847.

Hill, R. J.; Canterford, J. H.; and Moyle, F. J. 1982. New data for landsfordite. Mineral. Mag. 46:453–457.

Hull, H., and Turnbull, A. G. 1973. A thermochemical study of monohydrocalcite. Geochim. Cosmochim. Acta 57:3533–3554.

Jiménez-López, C.; Caballero, E.; Huertas, F. J.; and Romanek, C. S. 2001. Chemical, mineralogical and isotopic behaviour, and phase transformation during the precipitation of calcium carbonate minerals from intermediate ionic solution at 25°C. Geochim. Cosmochim. Acta 65:3219–3231.

Kangal, O.; Firat, C.; and Güney, A. 2005. Flotation of unusual carbonates: huntite and hydromagnesite. Mineral. Eng. 18:631–634.

Kazakov, A. V.; Tikhomirova, M. M.; and Plotnikova, V. I. 1959. The system of carbonate equilibria. Int. Geol. Rev. 1:1–39.

Kinsman, D. J. 1967. Huntite from a carbonate-evaporite environment. Am. Mineral. 52:1332–1340.

Königsberger, E., and Gamsjäger, H. 1992. Solid-solute phase equilibria in aqueous solution. VII. A re-interpretation of magnesian calcite stabilities. Geochim. Cosmochim. Acta 56:4095–4098.

Königsberger, E.; Königsberger, L. C.; and Gamsjäger, H. 1999. Low-temperature thermodynamic model for the system Na_2CO_3-$MgCO_3$-$CaCO_3$-H_2O. Geochim. Cosmochim. Acta 63:3105–3119.

Lanas, J., and Alvarez, J. I. 2004. Dolomitic lime: thermal decomposition of nesquehonite. Thermochim. Acta 421:123–132.

Langmuir, D. 1965. Stability of carbonates in the system MgO-CO_2-H_2O. J. Geol. 73:730–754.

Lippmann, F. 1973. Sedimentary carbonate minerals. New York, Springer.

Menzel, H., and Brückner, A. 1930. Studien an kohlensauren Magnesiumsalzen. I. Basische Magnesiumcarbonate. Z. Elektrochem. 36:63–87.

Morse, J. W., and Casey, W. H. 1988. Ostwald processes and mineral paragenesis in sediments. Am. J. Sci. 288:537–560.

Mucci, A., and Morse, J. W. 1983. The incorporation of Mg^{2+} and Sr^{2+} into calcite overgrowths: influence of growth rate and surface composition. Geochim. Cosmochim. Acta 47:217–233.

Pierantozzi, R. 1993. Carbon dioxide. *In* Kroschwitz, J. I., and Howe-Grant, M., eds. Kirk-Othmer encyclopedia of chemical technology (4th ed.). Vol. 5. New York, Wiley, p. 35–53.

Pokrovsky, O. S. 1998. Precipitation of calcium and magnesium carbonates from homogeneous supersaturated solutions. J. Cryst. Growth 186:233–239.

Queralt, I.; Juliá, R.; Plana, F.; and Bischoff, J. L. 1997. A hydrous Ca-bearing magnesium carbonate from playa lake sediments, Salines Lake, Spain. Am. Mineral. 82:812–819.

Raade, G. 1970. Dypingite, a new hydrous basic carbonate of magnesium, from Norway. Am. Mineral. 55:1457–1465.

Reddy, M. M., and Wang, K. K. 1980. Crystallization of calcium carbonate in the presence of metal ions. I. Inhibition by magnesium ion at pH 8.8 and 25°C. J. Cryst. Growth 50:470–480.

Russell, M. J.; Ingham, J. K.; Zedef, V.; Maktav, D.; Sunar, F.; Hall, A. J.; and Fallick, A. E. 1999. Search for signs of ancient life on Mars: expectations from hydromagnesite microbialites, Solda Lake, Turkey. J. Geol. Soc. Lond. 156:869–888.

Scheetz, B. E., and White, W. B. 1977. Vibrational spectra of the alkaline earth double carbonates. Am. Mineral. 62:36–50.

Stamatakis, M. G. 1995. Occurrence and genesis of huntite-hydromagnesite assemblages, Kozani, Greece:

important new white fillers and extenders. Trans. Inst. Mining Metal. 104:B179–B185.

Stanger, G., and Neal, C. 1994. The occurrence and chemistry of huntite from Oman. Chem. Geol. 112: 247–254.

Stipp, S. L. S. 1999. Towards a conceptual model of the calcite surface: hydration, hydrolysis, and surface potential. Geochim. Cosmochim. Acta 63:3121–3131.

Walling, E. M.; Rock, P. A.; and Casey, W. H. 1995. The Gibbs energy of formation of huntite, $CaMg_3(CO_3)_4$, at 298 K and 1 bar from electrochemical cell measurements. Am. Mineral. 80:355–360.

White, W. B. 1974. The carbonate minerals. *In* V. C., Farmer, ed. The infrared spectra of minerals. Mineral. Soc. Monogr. 4:227–284.

Zachmann, D. W. 1989. Mg-carbonate deposits in freshwater environments. *In* Möller, P., ed. Magnesite: geology, mineralogy, geochemistry, formation of Mg-carbonates. Monograph Series on Mineral Deposits. Vol. 28. Berlin, Bornträger, p. 61–94.

Queries

1. In the sentence beginning "Infrared analyses," the abbreviation ATR has been deleted because it is not used again in the article.